Comparative studies of the nonlinear effects occurring when highly charged projectiles collide with hydrogen, a free electron gas, and a harmonic oscillator

J. E. Miraglia and M. S. Gravielle
Instituto de Astronomía y Física del Espacio, Casilla de Correo 67, Sucursal 28, 1428 Buenos Aires, Argentina
(Received 16 May 2005; published 26 October 2005)

We calculate the nonlinear effects that appear at the level of the stopping cross section when heavy bare projectiles collide with both atomic hydrogen and a free electron gas. Calculations are carried out by using distorted-wave methods. For hydrogen targets we employ the continuum-distorted-wave eikonal initial-state approximation, while for the free electron gas we use the Coulomb-Lindhard approach. Results are compared with exact results for the quantum harmonic oscillator target. Ratios to the first-order stopping are analyzed in detail and their structures are interpreted in terms of Padé approximants. We also investigate the dependency of the stopping ratios on the impact parameter.

DOI: 10.1103/PhysRevA.72.042902 PACS number(s): 34.50.Bw, 34.50.Dy, 34.50.Fa

I. INTRODUCTION

It is well known that when a heavy projectile of charge Z_P penetrates matter at a high velocity v, the stopping power behaves as Z_P^2. However, as the velocity decreases, nonlinear terms, i.e., the ones behaving as Z_P^j with $j \geqslant 3$, become important. The calculation of these terms has been the subject of numerous publications and excellent summaries can be found in the literature [1–3].

For a fast heavy projectile moving through an *idealized* random medium, the energy loss per unit path length, also called stopping power cross section, is generally written as

$$S = \frac{\omega_0^2 Z_P^2}{v^2} L, \quad L = \sum_{n=0}^{+\infty} Z_P^n L_n, \tag{1}$$

where ω_0 is a natural frequency, which is defined in accord with the considered medium. If the medium is a free electron gas (FEG), ω_0 is defined as the plasmon energy ω_p, if the target is an atom, ω_0 is the mean excitation energy ω_i, and if the target is a harmonic oscillator (HO), then ω_0 is simply the oscillatory frequency. For these two latter cases, the density of targets should also be included in S. In Eq. (1), L is the stopping number, whose first term—the primary stopping number—reads $L_0 = \ln(2v^2/\omega_0)$.

For our purpose, it is convenient to re-write Eq. (1) in terms of the Sommerfeld parameter $a = Z_P/v$, by defining the ratio

$$R = S \frac{v^2}{\omega_0^2 Z_P^2 L_0} = \sum_{n=0}^{+\infty} B_{n+2} a^n, \tag{2}$$

where the B_j factors do not depend on Z_P, and $B_2 = 1$. The factor B_3, here called the relative Barkas correction factor, provides the Z_P^3-correction term [4,5] to the stopping power. The next factor, B_4, determines the Z_P^4-correction term of the stopping and it was introduced by Bloch [6]. The factor B_3 has been largely investigated for the three targets considered here—FEG, atomic hydrogen, and HO. For a FEG, the Z_P^3 contribution was calculated in the context of the many-body perturbation theory without exchange [7–10], while for atomic hydrogen and HO targets, the factor B_3 was simply derived from the second Born approximation [11,12].

For high impact velocity, the behavior of the Barkas and Bloch correction factors has attracted a great deal of attention. For $v \to +\infty$, Lindhard derived the following expressions [Eqs. (15) and (16) of Ref. [5]]: $B_{3,4} \to B_{3,4}^{(\infty)}$, with

$$B_3^{(\infty)} = \frac{3\pi\omega_0}{2v^2}, \quad B_4^{(\infty)} = -\frac{1.202}{\ln(2v^2/\omega_0)}. \tag{3}$$

This high-energy limit has been recently reexamined within the classical scheme [13], proving to be accurate when it was compared with a set of experimental data of channeled fast ions, as reported by Araujo *et al.* [14,15].

In spite of the efforts devoted to evaluate the B_3 factor, the Barkas term is not enough to describe the energy loss at intermediate velocities or for large Z_P, where higher-order Born terms are required [16]. If only the Barkas contribution is included, the calculation yields unacceptable negative values of stopping when $Z_P \to -\infty$. In a similar manner, calculations including only the Bloch and Barkas contributions provide negative values of the stopping in both limits, as $Z_P \to \pm\infty$, because $B_4 < 0$.

In this paper we report stopping cross sections for bare ions colliding with FEG and atomic targets at intermediate and high impact velocities. Results are obtained by using distorted-wave methods which take into account, albeit in an approximate way, *all orders* in Z_P. For the FEG we employ the Coulomb-Lindhard (CL) [17] approximation, while for atomic targets we use the well-established continuum distorted-wave eikonal initial-state (CDW) [18,19] approach. The CL approximation is a distorted-wave method based on the impulse approximation. It tackles the many-body problem that arises when a fast bare ion penetrates a FEG, including nonlinear effects in the projectile charge and collective modes [17]. In a similar fashion, the CDW describes higher perturbative terms for single ionization of atomic targets by impact of bare projectiles. CDW cross sections for large Z_P were studied in detail and compared with the experiments by Gilbody [20].

Present distorted-wave results will be compared, when possible, with exact calculations for HO targets extracted from Ref. [21]. In the last years, the HO has become a sort of wild card which has been used to simulate targets ranging from a FEG to any atom. As pointed out by Mikkelsen and Flyvberg [21], although attractive, the HO is by no means an exact atomic model. For example, the HO does not hold the charge exchange process, which represents an important mechanism of energy loss at low velocities. It does not even take into account many-body collective excitations, as observed in a FEG. Anyway, there is a huge amount of literature devoted to the HO: its perturbative expansion in term of Z_P [12,16,22,23], its classical solution [13,24], and its exact numerical evaluation [21].

The questions that this work intends to solve are the following. First, to what extent can both distorted-wave methods—the CL and CDW approaches—reproduce previous predictions for Barkas and Bloch terms? And second, how similar are CL and CDW stopping cross sections to each other, and both to the exact HO one, as a function of the projectile charge? To answer these issues, we will report results for two different targets: Al FEG and hydrogen in its ground state. This comparison is not arbitrary because both targets have very similar associated oscillator frequency ω_0. Following Cabrera-Trujillo [25], for H($1s$), $\omega_i \approx \langle r^2 \rangle^{-1/2} = 0.577$ a.u., which is very near to the plasmon energy $\omega_p = 0.566$ a.u. of Al. For the HO target we will resort to the exact calculation of Ref. [21] for $2v^2/\omega_0 = 10$ a.u. Therefore if we consider the same oscillation frequency $\omega_0 = 0.57$, the impact velocity is then $v = 1.68$ a.u.

It is important to mention that we will deal just with bare projectiles, while the *measured* stopping cross sections involve the different charge states of the projectile. Capture processes will not be considered here. Atomic units are used along the work.

II. BASIC DEFINITIONS

We consider bare projectiles, with charge Z_P, impinging with velocity v on two different targets: an Al FEG and atomic hydrogen in its ground state. For Al FEG, the process can be schematically represented by

$$Z_P + \mathrm{Al(FEG)} \rightarrow Z_P + \mathrm{Al(FEG)}^*, \tag{4}$$

where the asterisk indicates that the FEG ends in an excited or ionized state. We employ the CL approximation [17] to evaluate the energy loss per unit path, $S_{\mathrm{Al}}^{\mathrm{CL}}$, associated with this reaction. In order to compare with Eq. (2), we introduce the ratio

$$R_{\mathrm{Al}}^{\mathrm{CL}} = \frac{S_{\mathrm{Al}}^{\mathrm{CL}}}{S_{\mathrm{Al}}^{L}}, \tag{5}$$

where S_{Al}^{L} represents the first-order stopping cross section, depending on Z_P^2, as calculated by Lindhard [26] and Ritchie [27].

In similar way, the ionization of the hydrogen atom can be represented as

$$Z_P + \mathrm{H}(1s) \rightarrow Z_P + e + \mathrm{H}^+. \tag{6}$$

The corresponding stopping cross section, $S_{\mathrm{H}}^{\mathrm{CDW}}$, is calculated here by using the CDW method [18,19]. The first-order term, S_{H}^{B}, proportional to Z_P^2, is evaluated within the first-order Born approximation. Then, the ratio defined by Eq. (2) is expressed as

$$R_{\mathrm{H}}^{\mathrm{CDW}} = \frac{S_{\mathrm{H}}^{\mathrm{CDW}}}{S_{\mathrm{H}}^{B}}. \tag{7}$$

From the exact numerical result [21], we have extracted the ratio R_{HO} for the virtual case

$$Z_P + \mathrm{HO} \rightarrow Z_P + \mathrm{HO}^*. \tag{8}$$

In all cases, we expect the perturbative limit to hold, namely, $R_{\mathrm{Al}}^{\mathrm{CL}}$, $R_{\mathrm{H}}^{\mathrm{CDW}}$, $R_{\mathrm{HO}} \rightarrow 1$ as $a \rightarrow 0$.

III. RESULTS

To calculate the ratios $R_{\mathrm{H}}^{\mathrm{CDW}}$ and $R_{\mathrm{Al}}^{\mathrm{CL}}$, defined by Eqs. (5) and (7), respectively, we have developed two different codes. In the case of ionization of hydrogen, the calculation of the CDW is standard and simple [18,19]. It requires a four-dimensional numerical integration of a positive quantity, which involves hypergeometric functions. Relative errors were set to be much less than 0.1%. For the penetration of ions in the FEG the calculation of the CL approximation is far more complicated. The CL approach [17] involves a five-dimensional numerical integral of a complex and very-oscillatory function, which includes hypergeometric functions. Two major improvements have been made to our original code of Ref. [17]. First, we have used the fact that (in the notation of Ref. [17]) $\mathcal{K}^- = \mathcal{K}^{+*}$, which reduces almost half the computing time [28]. And second, we built a subroutine for specific values of the argument of the hypergeometric function in terms of the digamma function [see Eq. (15.3.11) of Ref. [29]]. In spite of these modifications, our CL code can only provide results with less than 1% of relative error, within a reasonable CPU time. The CL expression requires an effective charge to invoke the self-consistency [17]. As in the previous work, the charge has been chosen to be $Z_P \mathrm{Re}[1/\epsilon_M(q,0)]$, where q is the momentum transfer and ϵ_M is the Mermin-Lindhard dielectric function.

Al FEG is described with a Wigner-Seitz radius $r_s = 2.07$ a.u. (plasmon energy $\omega_P = 0.566$ a.u). and with a lifetime $\lambda = 0.0375$ a.u. For both targets, Al FEG and atomic hydrogen, we will report results for Sommerfeld parameters $a = Z_P/v$ within the range $-2 \leqslant a \leqslant 2$, and for impact velocities $v \gtrsim 2$, to be sure that distorted-wave methods work adequately. Of course, projectiles with $Z_P < -1$ have no physical meaning, but their calculation is necessary to evaluate perturbative series.

A. Stopping cross sections

We start the analysis by comparing our results with available experiments for antiproton and negative muon impact. We have considered these negative ions as projectiles to discard capture channels, not included in our calculations.

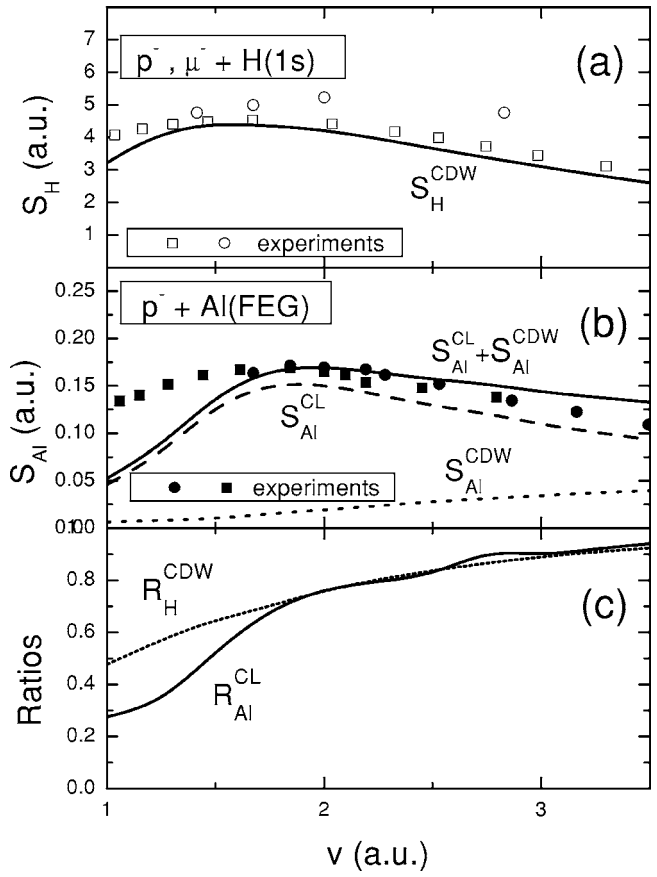

FIG. 1. (a) shows the stopping cross section per atom for negative ions on molecular hydrogen. Empty square, experiments for μ^- impact and empty circles, experiments for p^- from Agnello *et al.* [30]. Solid line the CDW calculation for atomic hydrogen. (b) displays the stopping cross section per unit path length for antiproton impact on Al target as a function of the projectile velocity. Dashed line $S_{\mathrm{Al}}^{\mathrm{CL}}$, FEG contribution; dotted line $S_{\mathrm{Al}}^{\mathrm{CDW}}$ contribution of the Al inner shells ($2s$ and $2p$); and solid line, the sum. Full circles and squares experiments from Moeller *et al.* [31]. (c) displays the theoretical ratios $R_{\mathrm{Al}}^{\mathrm{CL}}$ and $R_{\mathrm{H}}^{\mathrm{CDW}}$ as introduced in the text.

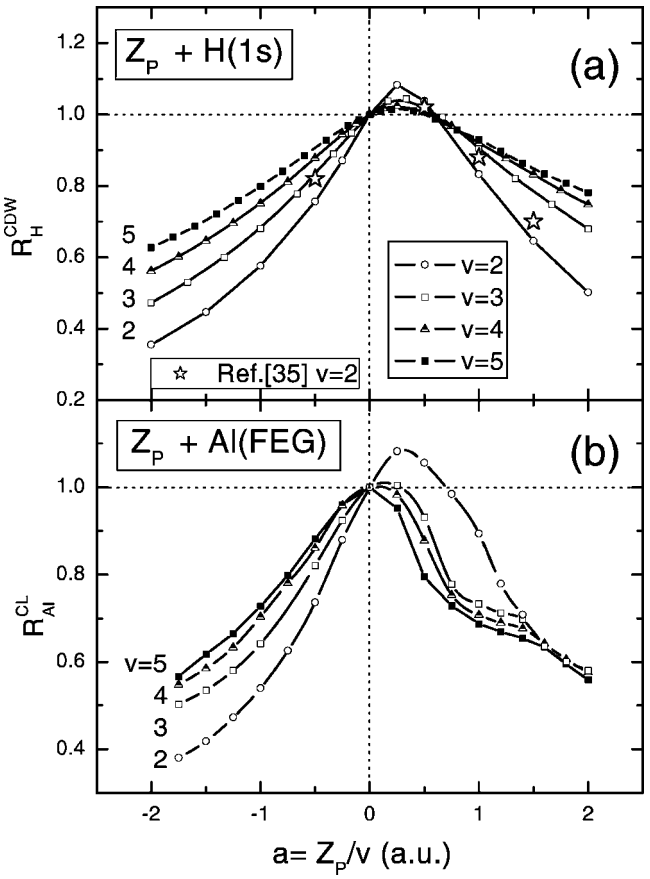

FIG. 2. Upper figure displays the ratio $R_{\mathrm{H}}^{\mathrm{CDW}}$ as a function of the Sommerfeld parameter a for different impact velocities, as indicated. Empty star symbols, close coupling results reported by Schiwietz [35]. Similarly, the lower figure shows the ratio $R_{\mathrm{Al}}^{\mathrm{CL}}$.

In Fig. 1(a) energy-loss experiments for antiprotons and negative muons impinging on H_2 are compared with our $S_{\mathrm{H}}^{\mathrm{CDW}}$ values. For atomic hydrogen, CDW results follow the tendency of the experiments. However, this agreement should be taken with caution because the experimental target is molecular, not atomic, hydrogen, and the excitation channel is not included in the theory.

In Fig. 1(b) we display two sets of energy-loss experiments for antiprotons moving in Al, as a function of the impact velocity. In order to compare our results with the experimental data, we need to add FEG and inner-shell contributions. We calculate the energy loss per unit path originated by ionization from the $2s$ and $2p$ shells of Al by using the CDW approximation, noted as $S_{\mathrm{Al}}^{\mathrm{CDW}}$. The total stopping cross section, $S_{\mathrm{Al}}^{\mathrm{CL}}+S_{\mathrm{Al}}^{\mathrm{CDW}}$, is in very good agreement with experimental values for $v \gtrsim 1.8$ a.u. Below this velocity, which is of the order of twice the Fermi velocity of the FEG, the CL approximation fails, as a consequence of including the impulse hypothesis. At low energies the stopping is known to increase linearly with v, and the screening plays a very important role [32,33]. For antiprotons moving at low velocities the stopping can be calculated by using an effective screened potential in the momentum-transfer cross section [34].

A very interesting point is shown in Fig. 1(c), where we plot together the theoretical ratios $R_{\mathrm{H}}^{\mathrm{CDW}}$ and $R_{\mathrm{Al}}^{\mathrm{CL}}$ for $Z_P=-1$, as a function of the projectile velocity. The coincidence between both theories for $v \gtrsim 1.8$ a.u. is impressive. It demonstrates the total equivalence at a level of the energy-loss cross section of the H($1s$) and Al (FEG) targets, as posed by the relation of Cabrera-Trujillo [25].

Figures 2(a) and 2(b) display the ratios $R_{\mathrm{H}}^{\mathrm{CDW}}$ and $R_{\mathrm{Al}}^{\mathrm{CL}}$, respectively, as a function of the parameter $a=Z_P/v$ for different velocities ($v=2$, 3, 4, and 5 a.u.). Similarities in the shape of the curves for FEG and H($1s$) targets are again remarkable. We considered the agreement of $S_{\mathrm{H}}^{\mathrm{CDW}}$ with experiments reported in Ref. [20] as an indication of the reliability of the CDW theory in the considered energy region. Further, in Fig. 2(a) we have included the numerical results for $v=2$ derived by Schiwietz [35] by using an atomic close-coupling calculation. Such results display good agreement with our CDW values. For strong distortions ($a \gtrsim 1$ a.u.) the CL approximation presents a small oscillatory pattern, also observed in Fig. 1(c), which might be a deficiency of the approximation.

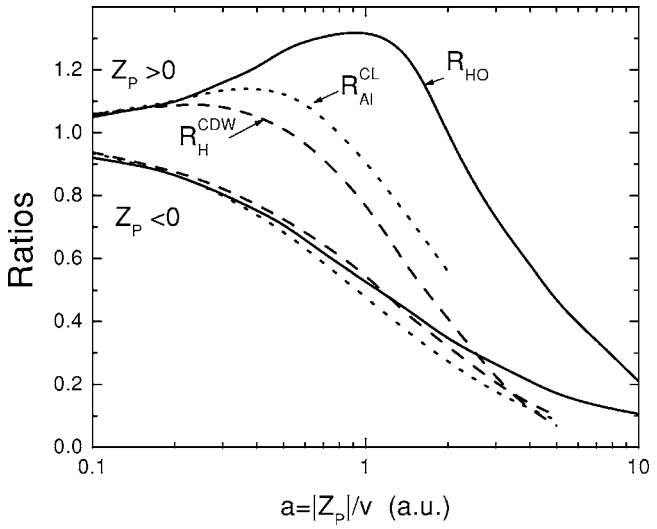

FIG. 3. The ratios of the calculated stopping with respect to their first order for $v=1.68$ as a function of the Sommerfeld parameter. In the solid line labeled with R_{HO} we plot the results reported by Mikkelsen *et al.* [21] for the harmonic oscillator; in dotted line, labeled with $R_{\mathrm{Al}}^{\mathrm{CL}}$, for charged bared ions on Al FEG; and in dashed line labeled with $R_{\mathrm{H}}^{\mathrm{CDW}}$, the continuun distorted wave for atomic hydrogen targets.

Since the HO target has been largely used to evaluate nonlinear contributions to energy loss, before proceeding, it is convenient to compare present ratios with *exact* calculations for the HO target. In Fig. 3, we plot $R_{\mathrm{H}}^{\mathrm{CDW}}$ and $R_{\mathrm{Al}}^{\mathrm{CL}}$ together with the *exact* ratio for the HO target, R_{HO}, as reported in Ref. [21] for $2v^2/\omega_0=10$ a.u. The associated impact velocity is $v=1.68$ a.u., which is not large enough to fully trust on the distorted-wave methods used here. We observe that for $Z_P<0$ the ratios corresponding to the three targets—Al FEG, atomic hydrogen, and HO—behave much alike. Some differences arise for $Z_P>0$, especially when the CL and CDW ratios are compared with the HO values. It would be indicative of the importance of the capture channel when the velocity decreases.

B. Series expansions

We are interested in evaluating the relative correction factors B_n, associated with the expansion of the ratio R in terms of the Sommerfeld parameter a, as given by Eq. (2). We have found that the direct polynomial interpolation of the numerical results $R_{\mathrm{H}}^{\mathrm{CDW}}$ and $R_{\mathrm{Al}}^{\mathrm{CL}}$, shown in Fig. 2, is not reliable to determine the B_n factors. For example, nine numerical values of the ratio R in the range $a\in[-1,1]$ give rise to a polynomial, which behaves (wrongly) as a^8 for large values of a. This asymptotic behavior does not satisfy the high-charge limit.

To include the experimentally observed saturation effect we resorted to Padé approximants, which allows us to obtain an interesting mathematical insight about nonlinear contributions. By using the Padé $[N,N+2]$ approximant we can write Eq. (2) as follows:

$$R\approx R^{[N,N+2]}(a)=\frac{\sum_{n}^{N}P_n a^n}{\sum_{m=0}^{N+2}Q_m a^m}, \tag{9}$$

with $P_0=Q_0=1$, where the number N determines the order of the approximation. For Al (FEG), Eq. (9) implies that when a increases,

$$S_{\mathrm{Al}}^{\mathrm{CL}}\approx S_{\mathrm{Al}}^{L}R^{[N,N+2]}(a)\to\omega_p^2L_0\frac{P_N}{Q_{N+2}}, \tag{10}$$

which is a constant independent of Z_P, in agreement with the observed saturation phenomena. Similar expressions can be also derived for the other two targets, H($1s$) and HO.

The first Padé, corresponding to $N=0$, can be expressed in terms of the relative correction factors B_n as

$$R\approx R^{[0,2]}(a)=\frac{1}{1-B_3a+(B_3^2-B_4)a^2},$$
$$=\frac{\alpha_+\alpha_-}{(a-\alpha_+)(a-\alpha_-)}, \tag{11}$$

where

$$\alpha_\pm=\frac{B_3}{2}\pm\sqrt{B_4-\frac{3}{4}B_3^2} \tag{12}$$

are the poles of $R^{[0,2]}(a)$. The poles $\alpha_\pm$ are expected to be conjugated complex because the stopping cross section ratio R does not diverge for any value of the parameter $a=Z_P/v$. To examine this aspect we consider the high-energy limit, $v\to+\infty$, for which the Barkas and Bloch correction factors display closed expressions, as given by Eq. (3). In this limit case, the poles of $R^{[0,2]}(a)$ verify $\alpha_\pm\to\alpha_\pm^{(\infty)}$ with $\alpha_+^{(\infty)}=[\alpha_-^{(\infty)}]^*$, where

$$\mathrm{Re}[\alpha_+^{(\infty)}]\to\frac{1}{4.808}\frac{3\pi\omega_0}{v^2},\quad \mathrm{Im}[\alpha_+^{(\infty)}]\to\sqrt{\frac{1}{1.202}\ln\left(\frac{2v^2}{\omega_0}\right)}. \tag{13}$$

When the velocity increases, that is, as $a\to0$, $\mathrm{Re}[\alpha_+^{(\infty)}]$ approximates to zero very rapidly and the function $R^{[0,2]}(a)$ becomes a symmetric function. It means that the effect of the sign of the charge Z_P on the energy loss tends to disappear, and the Barkas correction becomes negligible. In addition, as $a\to0$, $\mathrm{Im}[\alpha_+^{(\infty)}]$ increases very slowly, determining the perturbative limit $R\to1$. It is important to note that our Padé [0,2] is built at the level of ratio of stopping cross sections; it is not developed from the Schwinger variational principle using trial wave functions, as it was recently developed by Nazarov *et al.* [36].

For the different considered targets, we use the Padé structure $R^{[0,2]}(a)$ to represent the stopping ratio by fitting the

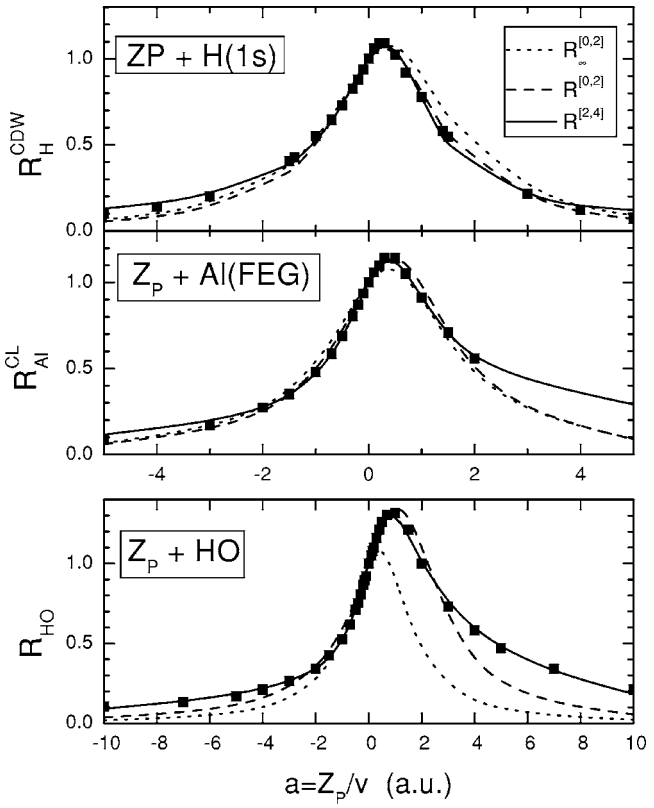

FIG. 4. Ratios for the three targets H(1*s*), Al (FEG), and HO as a function of the Sommerfeld parameter, for $v=1.68$. The symbols are the numerical results. For the case of the HO, the values were extracted from Mikkelsen *et al.* as reported in Ref. [21]. The dotted line shows the Padé [0,2] using the asymptotic values $\alpha_{1,2}^{\infty}$ given by Eq. (13). The dashed line shows the Padé [0,2] using the best fitted values of $\alpha_{1,2}$. The solid line shows the Padé [2,4] using the best fitted values α and β.

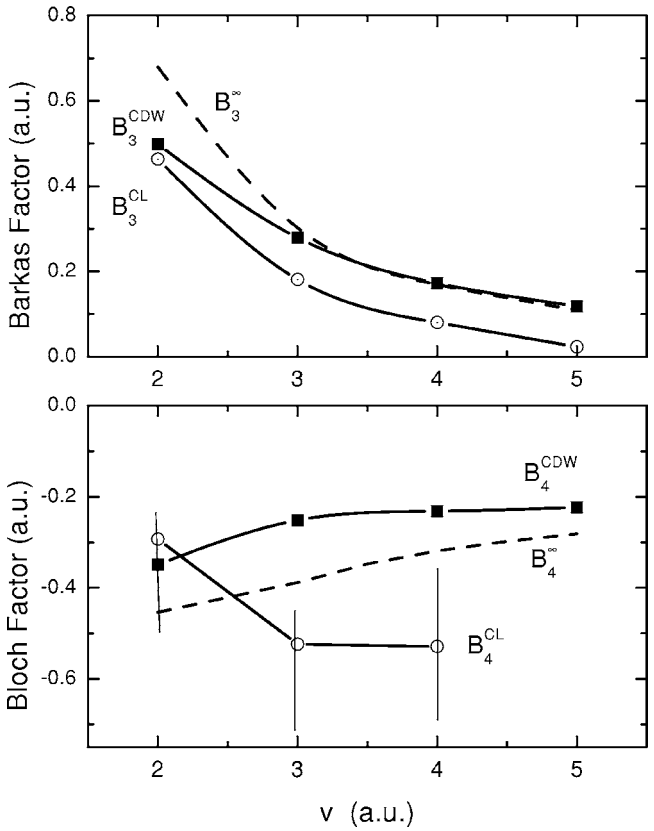

FIG. 5. Upper figure, Bloch factor B_4^{CDW} as given by Eq. (2) calculated by expanding the CDW energy-loss cross section in powers of the Sommerfeld parameter. Dashed lines, the asymptotic value B_4^{∞} given by Eq. (3). Lower figure, similar for the Barkas factor. Vertical lines represent the estimate error.

pole positions $\alpha_{\pm}$ from the theoretical values. Results for $R^{[0,2]}$ obtained from this fitting are displayed with the dashed line in Fig. 4. Full symbols represent present theoretical ratios, evaluated with the CDW and CL approximations for H(1*s*) and Al (FEG), respectively, and the exact values reported by Mikkelsen *et al.* [21] for the HO. The Padé approximant is a general and very powerful strategy. It allows us to combine saturation effects along with Barkas and Bloch corrections to derive two poles in the complex plane α_+ and α_-, which contain all the relevant information.

We also examine the use of the simple asymptotic values $\alpha_{\pm}^{(\infty)}$ of Eq. (13) to give $R_{\infty}^{[0,2]}(a)$. which is displayed in Fig. 4 with dotted lines. Again, the three different targets—H(1*s*), Al(FEG), and HO—are considered. In all the cases the asymptotic closed form $R_{\infty}^{[0,2]}$ predicts qualitatively the shape of the curve. Note that, paradoxically, the worst prediction corresponds to the HO target, from which asymptotic factors were extracted.

For higher N orders, we found it convenient to introduce roots by couples, that is, by using even numbers for N. The Padé [2,4] structure reads

$$R \approx R^{[2,4]}(a) = \frac{\prod_{j=1}^{4} \alpha_j \prod_{i=1}^{2} (a-\beta_i)}{\prod_{i=1}^{2} \beta_i \prod_{j=1}^{4} (a-\alpha_j)}, \tag{14}$$

where α_j and β_i are parameters derived by fitting the theoretical ratio R. For the three targets, $R^{[2,4]}(a)$ is also plotted in Fig. 4 with a solid line. It reproduces very accurately the distorted-wave and exact predictions. We found that $R^{[2,4]}(a)$ never becomes negative and it can be used with confidence for $a \to \pm\infty$.

After proving the success of Eq. (14) to represent the stopping cross section, we employ the fitted Padé [2,4] structure to derive Barkas and Bloch correction factors for Al (FEG) and H(1*s*) targets. To that end, we first calculate the Padé [2,4] approximant by fitting the CL and CDW results, shown in Fig. 2, in the range $a=[-1,1]$ a.u. And then, we expand it in a power series in terms of a. In this way, we derive the Barkas (B_3) and Bloch (B_4) factors, which are shown in Fig. 5 along with the asymptotic values $B_{3,4}^{(\infty)}$, given by Eq. (3). We have verified that the Padé [4,6] does not change appreciably the factors obtained with the Padé [2,4]. When the velocity augments, the agreement with the

asymptotic values is quite good for B_3^{CDW} and reasonable for B_4^{CDW} and B_3^{CL}. The factor B_4^{CL}, instead, behaves differently at high velocities, although it displays the appropriate sign and order. Within the CL approximation, used to evaluate the Al (FEG) target, the numerical procedure to determine the coefficients B_4^{CL} is not precise due to the uncertainty introduced by the numerical relative error (1%). The larger v, the nearer the ratio to unity, and so the larger the relative error. The estimated errors are displayed in the figure with vertical lines.

C. Impact parameter dependency

Several articles deal with the dependency of nonlinear contributions on the impact parameter ρ associated with the collision. Based on a HO target, Ashley *et al.* [37] argued that only large impact parameters contribute to the Z_P^3 correction, and introduced a lower limit for the impact parameter, $\rho_{\min} \approx 1$ a.u. (atomic radius). Later, Jackson and McCarthy [38] and Lindhard [5] modified slightly the value of $\rho_{\min}$. Mikkelsen *et al.* published a series of articles for the HO target, starting from the second order [22] and ending in the exact calculation [21] of the stopping in terms of the impact parameter. Examining the exact stopping for the HO target, they estimated $\rho_{\min} \approx Z_P/v^2$ only for $|a| = |Z_P/v| \gg 1$ a.u. For $|a| \approx 1$ a.u., the Barkas contribution was found to be relevant for small and intermediate values of the scaled magnitude $\rho\omega_0/v$.

In collisions with a quantum FEG, as considered within the CL approximation, electrons are described by totally extended plane waves. As a consequence, there is no quantity that can be identified with the impact parameter. For heavy ion-atom collisions, instead, it is possible to define an impact parameter ρ, measured with respect to the target nucleus. By using the eikonal approximation [39], we derive the impact-parameter distributions of the energy loss per unit path within the CDW and first-order Born approximations, $S_{\mathrm{H}}^{\mathrm{CDW}}(Z_P,\rho)$ and $S_H^B(Z_P,\rho)$, respectively. We have explicitly introduced the parameter Z_P in the notation to identify the charge of the bare ions impinging on H($1s$). This mathematical task involves an additional two-dimensional numerical integration, which is particularly laborious for large ρ values.

In order to separate the contributions of even (a^{2n}) and odd (a^{2n+1}) terms in the series given by Eq. (2), we define the following parity contributions:

$$P_{\mathrm{H}}^{\mathrm{even}}(Z_P,\rho) = \frac{S_{\mathrm{H}}^{\mathrm{CDW}}(Z_P,\rho) + S_{\mathrm{H}}^{\mathrm{CDW}}(-Z_P,\rho) - 2S_{\mathrm{H}}^{B}(Z_P,\rho)}{2S_{\mathrm{H}}^{B}(Z_P,\rho)},$$

$$P_{\mathrm{H}}^{\mathrm{odd}}(Z_P,\rho) = \frac{S_{\mathrm{H}}^{\mathrm{CDW}}(Z_P,\rho) - S_{\mathrm{H}}^{\mathrm{CDW}}(-Z_P,\rho)}{2S_{\mathrm{H}}^{B}(Z_P,\rho)}. \qquad (15)$$

Results for $v=2$ a.u. and for projectile charges $Z_P=1$, 2, and 3 are plotted in Fig. 6. From the figure we can undoubtedly state that even Z_P terms dominate the stopping cross section for small values of ρ, while odd terms are small in this impact parameter region. This behavior was also observed in closed coupling calculations at higher velocities [40]. For large impact parameters, even and odd parities give similar contributions to the stopping. These findings support the previous idea, based in the HO target, for which large ρ values essentially contribute to the Barkas correction. From Fig. 6 it is also concluded that the even contribution is important in the small impact-parameter range, where the stopping cross section is relevant.

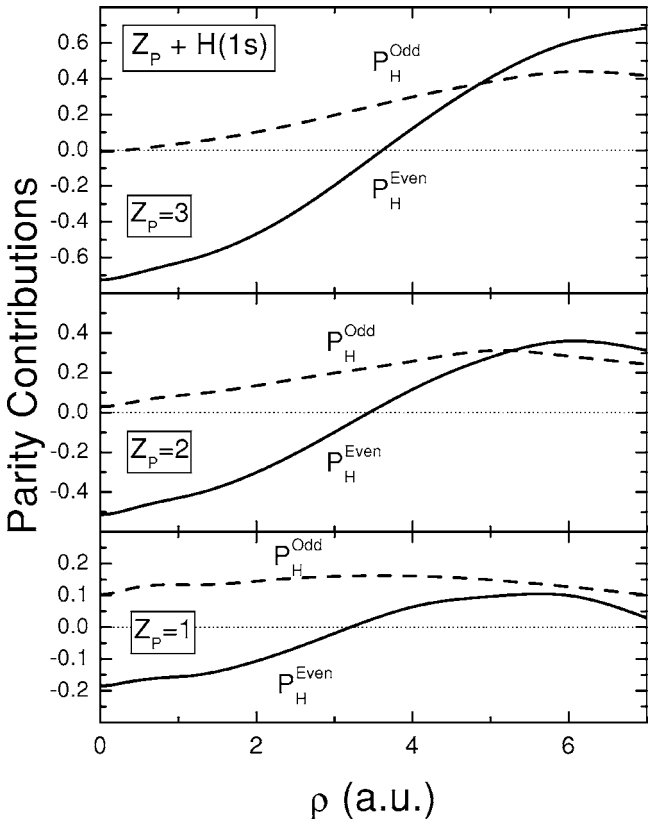

FIG. 6. Odd and even contributions defined in Eq. (15) for bare ions colliding with hydrogen in its ground state as a function of the impact parameter ρ for $v=2$. Values calculated with the CDW for three different projectile charges Z_P as indicated.

Finally, in Fig. 7 we compare the energy-loss distributions, as a function of the impact parameter, for idealized projectiles with $Z_P=\pm 1.68$ colliding with H($1s$) and HO targets, with velocity $v=1.68$ a.u. Both targets have similar frequencies ω_0. Even though the curves for H($1s$) display a sharper distribution than the corresponding to the HO target, the ratios with respect to first-order Born results become rather similar when they are plotted in terms of the universal parameter $\rho\omega_0/v$.

IV. SUMMARY AND CONCLUSIONS

We can now answer the two questions posed in the introduction. First, the distorted-wave methods (both the CL and CDW) do incorporate higher order in Z_P, including Barkas and Bloch corrections, but differing from each other, little for the Barkas factors and relatively large for the Bloch ones. Anyway, both targets give nearly the same ratios for large impact velocities. And second, for the case reported by

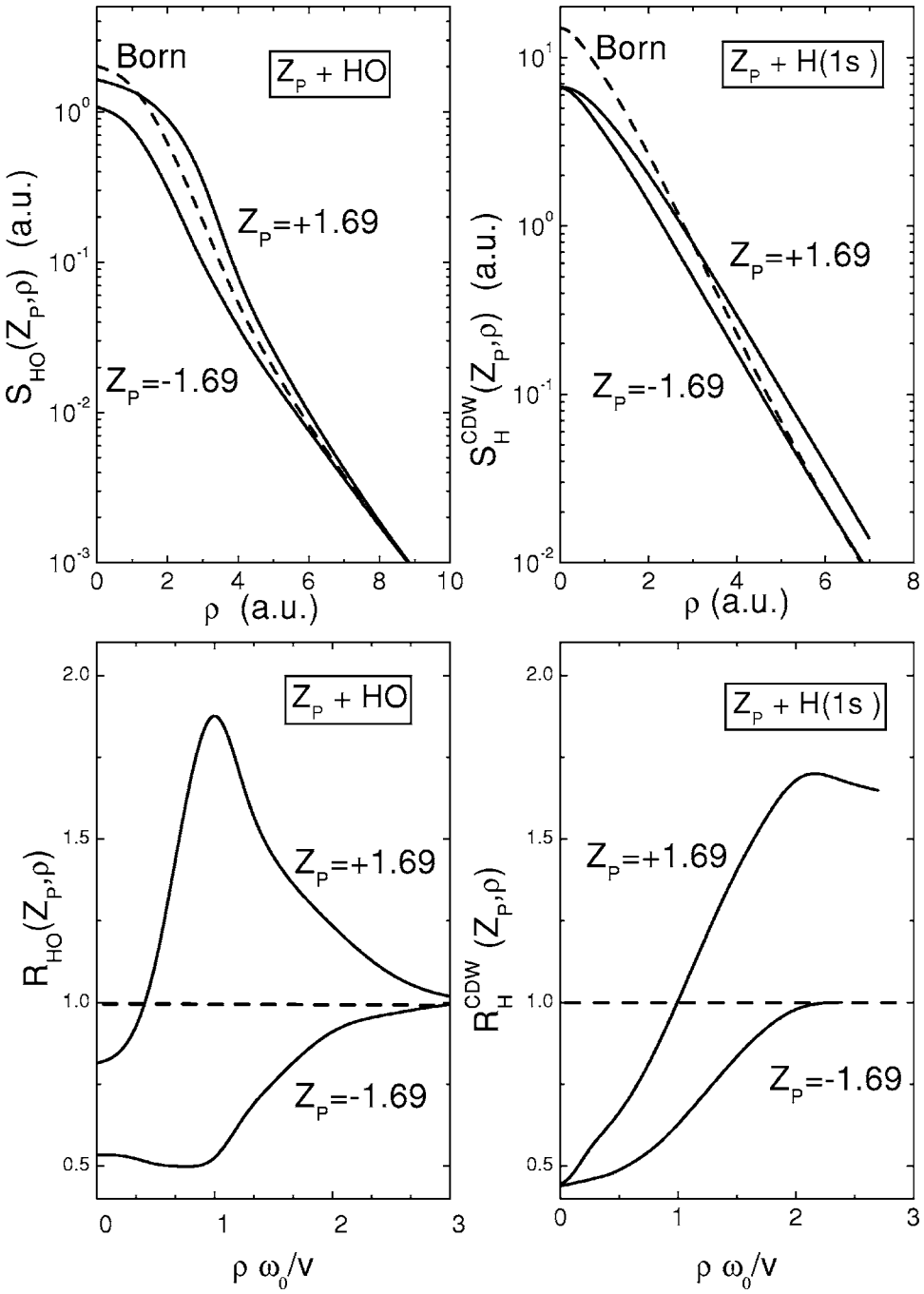

FIG. 7. Upper figures display stopping cross sections for $Z_P = \pm 1.69$ as a function of the impact parameter ρ for H($1s$) and HO as indicated. Lower figures show the corresponding ratios in terms of the scaled impact parameter.

Mikkelsen [21], at $v=1.68$, we find remarkable similarities among the three targets, viz. H, FEG, and HO, for $Z_P<0$, but some differences are observed for $Z_P>0$. The FEG results run very near to those of the H($1s$) target, and both run below the HO prediction for $a>1$. For $0\leqslant a<1$, the three targets run together warranting similar contribution to the Barkas effect. The capture channel, which is absent in the HO case, may play a role for atomic targets originating the differences found for $a>0$.

It is difficult to find a physical reason to support any similarity among the nonlinear terms for the different targets. For example, if we analyze the agreement for $Z_P<0$ to put aside the capture obstacle, it is clear that if such negative charges existed, the physics involved in the collision should be different. Why do both the FEG and H($1s$) targets give similar ratios to the HO (see Fig. 3)? This is puzzling. The numerical similarities between the FEG and H($1s$) targets [see Fig. 1(c)] is another interesting point to discuss. Although both have the binary channel, the FEG case has, in addition, the collective oscillation mode which contributes as importantly as the binary one. As a consequence, a plasmon peak appears in the differential energy-loss spectrum, which certainly is not present at all in the atomic spectrum. At this stage we should keep in mind that the CL approximation studied here is a distorted-wave method developed in the same spirit as the CDW for ionization. Perhaps the strong numerical similarities may be a consequence of the equal approach to the problems.

The output of the study of the present theoretical methods have two contradictory readings. On one hand, we can state that there are distorted-wave methods—such as the ones studied here—which provide adequate descriptions considering the real target under study, being either a FEG or an atom. And this is what we want to stress in this paper. But on the other hand, we cannot but admire those researchers who, using the HO model, unveil the core of the problem with very simple algebra, something that today illuminates our understanding of the numerical results.

ACKNOWLEDGMENTS

The authors wish to acknowledge illuminating discussions with D. Arbó, N. Arista, P. Grande, and M. Behar. This work was done with the financial support of CONICET, UBACyT, and ANPCyT of Argentina.

[1] J. F. Zieler, Appl. Phys. A: Mater. Sci. Process. **85**A, 1249 (1999), and references therein.
[2] N. R. Arista, Nucl. Instrum. Methods Phys. Res. B **195**, 91 (2002).
[3] L. L. Araujo, Ph.D. thesis, University of Porto Alegre, Brasil, 2004.
[4] W. Barkas, N. J. Dyer, and H. H. Heckman, Phys. Rev. Lett. **11**, 26 (1963).
[5] J. Lindhard, Nucl. Instrum. Methods **132**, 1 (1976).
[6] F. Bloch, Ann. Phys. **16**, 285 (1933); Z. Phys. **81**, 363 (1933).
[7] J. M. Pitarke, R. H. Ritchie, P. M. Echenique, and E. Zaremba, Europhys. Lett. **24**, 613 (1993).
[8] J. M. Pitarke, R. H. Ritchie, and P. M. Echenique, Phys. Rev. B **52**, 13883 (1995).
[9] D. G. Arbó, M. S. Gravielle, and J. E. Miraglia, Phys. Rev. A **62**, 032901 (2000).
[10] D. G. Arbó, M. S. Gravielle, and J. E. Miraglia, Phys. Rev. A **64**, 022902 (2001).
[11] C. H. Maier and H. J. Liehl, J. Phys. B **10**, 248 (1977).
[12] P. Sigmund and U. Haagerup, Phys. Rev. A **34**, 892 (1986).
[13] N. R. Arista, P. L. Grande, and A. F. Lifschitz, Phys. Rev. A **70**, 042902 (2004).
[14] G. de M. Azevedo, P. L. Grande, M. Behar, J. F. Dias, and G. Schiwietz, Phys. Rev. Lett. **86**, 1482 (2001).
[15] L. L. Araujo *et al.*, Phys. Rev. A **70**, 032903 (2004).
[16] H. H. Mikkelsen and H. Flyvbjerg, Phys. Rev. A **42**, 3962 (1992).
[17] J. E. Miraglia, Phys. Rev. A **68**, 022904 (2003).
[18] D. S. F. Crothers and J. F. McCann, J. Phys. B **16**, 3229 (1983).
[19] P. Fainstein, V. H. Ponce, and R. Rivarola, J. Phys. B **24**, 3091 (1991).
[20] H. B. Gilbody, Adv. At. Mol. Phys. **22**, 143 (1986).
[21] H. H. Mikkelsen and H. Flyvbjerg, Phys. Rev. A **45**, 3025 (1992).
[22] H. H. Mikkelsen and P. Sigmund, Phys. Rev. A **40**, 101 (1989).
[23] H. H. Mikkelsen, A. Meibom, and P. Sigmund, Phys. Rev. A **46**, 7012 (1992).
[24] E. R. Custidiano, F. J. Pérez de la Rosa, and M. M. Jakas, Phys. Rev. A **66**, 052902-1 (1992).
[25] R. Cabrera-Trujillo, Phys. Rev. A **60**, 3044 (1999).
[26] J. Lindhard, K. Dan. Vidensk. Selsk. Mat. Fys. Medd., **28** (No. 8) (1954).
[27] R. Ritchie, Phys. Rev. **114**, 644 (1959).
[28] D Arbó (private communication).
[29] M. Abramowitz and I. Stegun, *Handbook of Mathematical Functions* (Dover, New York, 1972).
[30] M. Agnello *et al.*, Phys. Rev. Lett. **74**, 371 (1995).
[31] S. P. Moller *et al.*, Phys. Rev. A **56**, 2930 (1997).
[32] I. Nagy and B. Apagyi, Phys. Rev. A **58**, R1653 (1998).
[33] N. R. Arista and A. F. Lifschitz, Phys. Rev. A **59**, 2719 (1999).
[34] I. Nagy, Nucl. Instrum. Methods Phys. Res. B **94**, 337 (1994).
[35] G. Schiwietz, Phys. Rev. A **42**, 296 (1990).
[36] V. U. Nazarov, S. Nishigaki, J. M. Pitarke, and C. S. Kim, Phys. Rev. B **71**, 113105 (2005).
[37] J. C. Ashley, R. H. Ritchie, and W. Brand, Phys. Rev. A **8**, 2402 (1973).
[38] J. D. Jackson and R. L. McCarthy, Phys. Rev. B **6**, 4131 (1972).
[39] Dz. Belkic, R. Gayet, and A. Salin, Phys. Rep. **56**, 279 (1979).
[40] P. L. Grande and G. Schiwietz, Nucl. Instrum. Methods Phys. Res. B **132**, 264 (1997).